AUTOMATED SEGMENTATION OF BLOOD VESSELS IN IMMUNO-STAINED WHOLE SLIDE IMAGES

Matthieu de Castelbajac[1]

[1]Department of Computer Science, Sorbonne Universite - under the supervision of Pr. Isabelle Bloch

1. INTRODUCTION

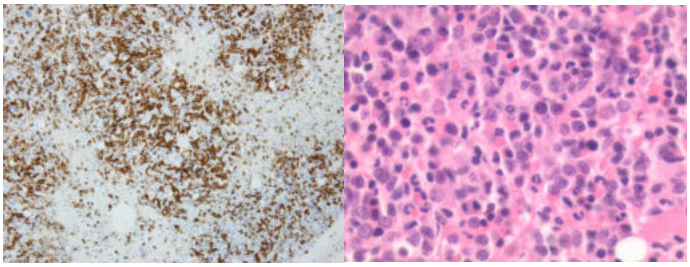

Figure 1: Anti-CD3 (left) and Hematoxylin-and-Eosin (H&E) (right) tiles from whole-slide images (WSI)[1]

Glioblastoma is the most common form of brain tumor, and is highly lethal.[2] And although immunotherapy brought promising results in fighting other aggressive cancers, glioblastoma has mostly been resisting it so far.[3] This failure is assumed to be multifactorial.[3] One of these factors could be related to the ill-explained unequal pervasiveness of cytotoxic T-lymphocytes (CTL) in the tumoral tissue. Whenever a tumor settles, it triggers angiogenesis, an abnormal growth of blood vessels around and inside the tumor to feed its cells. CTL then crawl out of these vessels to fight the tumor. And pathologists have observed that, for some vessels, CTL would crawl out of the blood vessels regularly, but that for some other, CTL would clot around the vessel. We wish to study this pervasiveness of the CTL around the blood vessels. But there is no easy way yet to analyze such cell spatial distribution. In order to identify and discriminate CTL from other surrounding cells, pathologists stain glass slides with anti-CD3 staining. CD3-positive, or brown shades, indicate CTL presence, whereas CD3-negative, or blue shades, appear for other types of cells. These slides are then digitized as whole-slide images (WSI) to undergo computer-based processing. There exist well-trained models along with comprehensive datasets to automatically segment cell nuclei on anti-CD3 staining.[4] But pathologists still have to perform manual segmentation of regions of interest beforehand, since most methods that can respond to this need are designed to work on the more common - and cheaper - Hematoxylin and Eosin staining (H&E), which purpose is to neatly recover cells nuclei, suitable for a much wider variety of studies. These steps are required to reduce the image size and remove artifacts that could hinder automated methods performances. And on top of it, they have to manually mark the blood vessels within these regions.

Manual segmentation is tiresome, time-consuming as well as prone to introduce intra- and inter-operator variability.[5] Hence, automated methods are really needed.

Hopefully, the development of computer-aided diagnosis brought many automated segmentation methods,[6] including several for blood vessel segmentation on WSI. Fully supervised methods do perform best, but they suffer several limitations. First, they are staining specific, with most of the networks being trained on standard H&E stained WSI.[7] They are also region or cancer specific, since both blood vessels and overall tissue appearances vary given the type of cancer.[7] Most of these use some filtering methods to select the areas to segment, then a convolutional network to adjust the segmentation masks or to discriminate blood vessels among different kinds of structures[7,8] But the last and probably most prevalent problem is the lack of data. Most of the studies proposing supervised methods rely on data commissioned from pathologists (which are not publicly available). But as we said, manual segmentation is time-consuming, and since WSI change in appearance given the type of cancer, getting the required amount of verified annotations is irrelevant – especially with glioblastoma for which data is relatively scarce for this is a rare cancer – and is not in the scope of this project.

There exist unsupervised methods that give good result as well,

and do not require as much data. Clustering based methods can perform well[9] for instance – relying either on k-means or mean-shift algorithms, where the latter is generally more robust and brings better results but is really computationally expensive.[10] But they have to assume that vessels shapes are not too heterogeneous to be clustered together. Though in reality we observe vessels with highly varying shapes, from very open and round interior, or lumen, to very thin lines with barely to completely invisible lumen. Other methods based on morphological segmentation work well, especially when relying on prior HSV decomposition[11],[1213],[14] but can require extensive parameter tuning. That being said, the vast majority relies on a different staining than anti-CD3, which is anti-CD31, anti-CD34 or anti-ERG, all targeting endothelial cells, or in other words, the blood vessels membrane, which makes them much more robust at spotting the vessels in the first place, and therefore eases the segmentation task.

Even more robust methods have been proposed to deal with both opened and closed vessels (with or without visible lumen)[12],[9].

A last type of method is just starting to be explored : staining transfer. That is, networks able to learn how to synthesize WSI with expensive staining method from more general ones (mostly H&E) from pairs of registered slides give great results.[15] But not only does the training require data, it also requires costly preparation, as staining cannot be done one after the other on the same slide without strongly damaging the structures ; so that it actually requires twice the amount of slides, prepared in pairs, finely separated in the tissue, with extensive registration between the two.

Taking into account the scarcity of anti-CD3-stained WSI for glioblastoma, we propose to adapt unsupervised methods to those, able to segment blood vessels. That being said, anti-CD3 staining does not reveal blood vessels membrane as anti-C31 does. However, we use the following shortcut, coming back to the roots of the experiment. Indeed, considering the need to analyze the surrounding CTL spatial distribution, we can ignore in our case all the blood vessels that do not feature nearby CTL – which significantly reduces the variability of vessels to detect. That leaves two cases. Either the remaining blood vessels have no lumen and are clotted with CTL, and in this case, we can treat the clot as the vessels' borders. Either it has a clear lumen with surrounding CTL, and we can try and detect the CTL and then more finely segment the lumen, both conditions not being mutually exclusive in a given WSI. Since the end goal is to detect all blood vessels though, we also try to segment vessels from their lumen only.

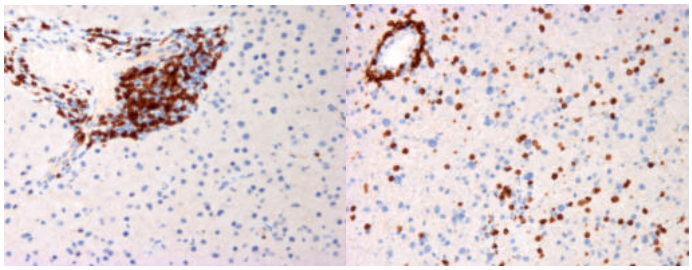

Figure 2: CD3 patches : CTL are clotted around the vessel (left), CTL infiltrate the tissue (right)

2. RELATED WORK

Previous unsupervised automated blood vessel segmentation methods were typically developed on anti-CD31-stained or anti-CD34-stained WSI, where blood vessels membrane are highlighted in brown shades. To deal with the encountered variability of blood vessels lumen shapes, *Fernández-Carrobles & al*[12] proposed a dual pipeline able to segment both *opened* and *closed* vessels, respectively meaning vessels with clearly visible lumen or indistinguishable ones (we keep using the same terminology thereafter). First, the method locates and segment closed vessels by decomposing the image given its hue, saturation and value channels (H,S,V). Brown shades in the WSI are highly saturated compared to pale blue shades for other cells, so that CD31-positive endothelial cells can be somewhat isolated on a thresholded S channel. Since there is only one thing to segment over a background here, being the blood vessels contours, it makes perfect sense to work on a binary mask. To enhance this mask, the method includes a succession of morphological operations, erosion and dilation. Regarding segmentation, binary erosion decreases components size based on a structuring element with a given size. That is, considering an image – or an component – I and a structuring element S of a given size then the binary erosion of I by S is defined as follow, where $S(i, j)$ is the structuring element centered at the pixel (i, j).

$$I \ominus S = \{(i, j) \mid S(i, j) \in A\} \tag{1}$$

On the other hand, binary dilation increases components size – hence the names – to such extent as defined by the size of the structuring element. Dilation is thus the complementary operation of the erosion and a definition of the binary dilation of I by S could be given as follows.

$$I \oplus S = \{i + j \mid x \in I, j \in S\} \tag{2}$$

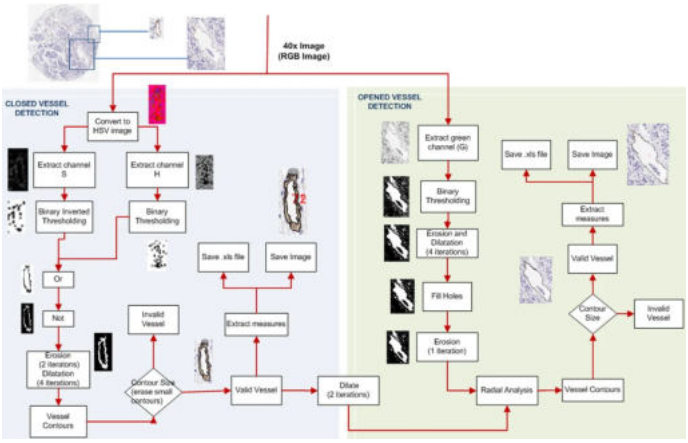

Figure 3: Vessel segmentation process:[12] Segmentation based on HSV colour model (left) and radial algorithm for detecting open vessels(right).

The second half of the method focuses on vessels with open lumen. To extract the lumen shape, it uses the green channel of the RGB decomposition, as it appears more clearly in this one, and uses edge detection.[12] The mask enhancement process is similar : the erosion removes small holes nearby and the dilation reconstructs the vessel back. Its application gave interesting results, especially since it is able to segment both types of vessels on a given image, coming a loss in consistency, though.

The method recently proposed by *Bukenya & al* takes inspiration from the previous one.[9] Here, the image is also converted to HSV space. Then, a threshold based on distance on a k-means clustering is able to remove the background.[9] Also, small artifacts are removed based on component connectivity of small objects encompassing the 8-connectivity – that is, objects whose pixels can be chained either by directly by sharing edges, or by sharing corners. The minimum size is still defined by the author to match their data. In a similar fashion, erosion is also used to remove remaining artifacts while dilation is used to expand the remaining shapes. Note that the direct succession of an erosion and a dilation with the same structuring element is also called an opening and is defined as – in the binary case :

$$I \circ S = (I \ominus S) \oplus S \tag{3}$$

Although the following dilation can typically require a larger structuring element than the erosion to achieve good results.
In order to differentiate opened from closed vessels, the method relies this time on the Euler number, which is defined as the difference of the number of connected components and the number of holes. Such that if the Euler number associated to a given vessel

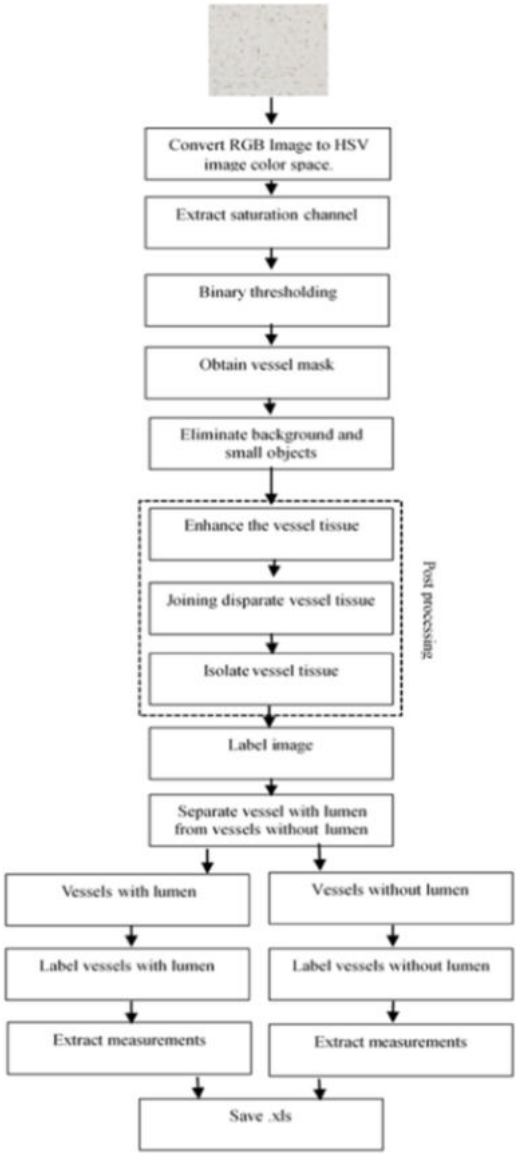

Figure 4: Vessel segmentation procedure[9]

is less than one, then the vessel has at least as much holes as it has connected components, and is considered as being opened, while the vessels whose Euler numbers are equal to one have less holes than they have connected components and are considered as being closed.[9]

3. METHOD

We adapted the previous works to our anti-CD3-stained WSI which came in the proprietary `.czi` format, along with manual segmentation masks reviewed by pathologists, for both blood vessels and regions of interest in a `TIF` format. Unfortunately, these annotations were not coming at the native resolution or coordinate system, so there was some registration to be done, to ensure further assessment. A raw WSI weight averages the couple of gigabytes. Needless to say it had to be downsampled, to the tenth in this case, to preserve details. Although an alternative solution would be to split the whole file into tiles to keep working at the native resolution – besides, this could be a way to improve the method later on. The downsampled slides were then clipped within the region masks.

Vessels do have drastic changes in appearance. They can be more or less surrounded with CTL, and have more or less visible lumen. And since the anti-CD3 staining is not nearly as good as anti-CD31 one at highlighting vessels boundaries, the method should be encompassing different cues to detect blood vessels. To that regard, we adapt both the opened and closed vessels distinction from the first method from *Fernández-Carrobles & al*, and the lumen retrieving through holes from the second method from *Bukenya & al.*.[9] On the opposite, we do not rely on HSV decomposition for we had trouble correlating saturation maxima with CTL presence, nor do we use edge detection but rather on other morphological operators.

(a) First, we normalize the WSI between 0 and 255 and extract the green channel.

(b) We then define bounding boxes to narrow the detection field. These can be define by two criteria. If there is enough CTL presence on the slide, we use these – which appear as global minima on the G channel – to define our bounding boxes, using a low pass threshold. Else, we seek global maxima instead with a high pass threshold as we directly target lumen. The resulting bounding boxes are then merged based on proximity to avoid redundancy.

(c) With CTL-based bounding boxes, we can focus on vessels boundaries first – which enables closed vessels detection. To do so, we perform an area opening on local minima followed by an area opening. The area opening is an opening that uses the max-tree representation with a predicate on component surface. Such that we can filter shapes that are either too small (artifacts, individual CTL) or too large (mainly erroneous masks due to threshold values). This step is directly followed with a combination of dilation and erosion operators to remove small holes. Then we look at the inverse mask. All remaining holes – which are now components – are simply taken as lumen and we call these derived lumen masks. And the method also returns vessels border masks. To also take closed vessels into account, the method returns the border masks as well.

(d) We add a last secondary branch to this method, in case of low CTL presence – to now spot open vessels directly through their visible lumen. We apply a high pass threshold instead, targeting maxima. From there, it appeared that the lumen luminosity was not standing out as much as in Fernández-Carrobles' study,[12] such that it was not possible to simply replicate the steps. And instead we found better results with morphological reconstruction. Morphological reconstruction by erosion is similar to basic morphological erosion, in the sense that low-intensity values will replace nearby high-intensity values. But in contrast, instead of the standard structuring element, it uses a mask, an image to limit the highest value of each pixel. We use a closing as a mask to preserve the lumen and perform the operation on the original image. This strengthens the difference between the lumen and the surrounding, so that we obtain clean contours. We can define the erosion in the general case as follow, expanding the binary case :

$$\forall x \in \mathbb{R}^n, E(I,B)(x) = inf\{I(y)|y \in B_x\} \tag{4}$$

with I an image and B a structuring element. During the reconstruction, the image is essentially eroded at each iteration until it converges with its closing. The result is we have a sharp contour of the lumen. Note that it should be possible to set an edge detector directly from either the reconstruction or the closing step to follow more closely the steps of the previous study, and could be a way to improve the method later on.

Next, we show the outline of the complete method.

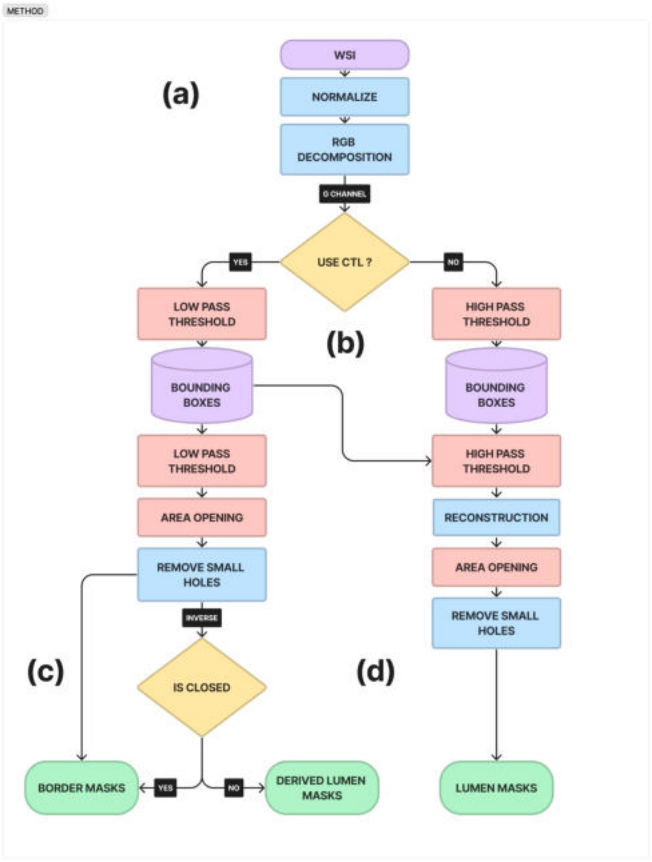

Figure 5: Flow chart of the complete method

Of course, several operators (*in red above*) are subject to parameter tuning. We use four of them, to be freely set by the user : a `LP_THRESHOLD` intensity value to perform low-pass threshold, `HP_THRESHOLD` factor of the local maximum and two `MIN_AREA` and `MAX_AREA` number of pixel values for area opening filtering.

Let us add that all morphological operations used here use disk as their structuring element, for the blood vessels lumen and borders to be retrieved are of relatively smooth shapes, with no specific orientation, that do not require hard edge detectors that are usually retrieved using square, diamonds or lines as structuring elements, depending on thinness and orientation, a priori.

4. RESULTS

We tested our method on four annotated and reviewed WSI scenes, that feature both opened and closed vessels, with and without nearby CTL. Since we only tested the method on such a limited amount of data, we provide a short qualitative per-slide analysis with a few examples, along with the total number of correctly or incorrectly detected vessels.

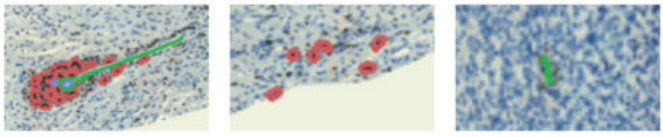

Figure 6: First scene samples. Borders in red, derived lumen in blue, lumen in purple and ground truth in green

The first scene is allegedly the hardest one to detect vessels in, since it combines all the pitfalls for our method : unstable stain values, high cell density, and closed vessels with low CTL presence. Hence, although the most visible vessels are detected, most are missed and we have a lot of false positive as well, as one can see in the center figure.

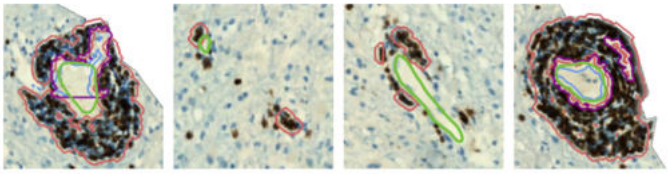

Figure 7: Second scene samples. Borders in red, derived lumen in blue, lumen in purple and ground truth in green

The second scene certainly represents an easy case. Diffusion is poor, and CTL are clearly distinguishable. Hence, vessels borders are easy to retrieve. Notice how for completely surrounded opened vessels, we do retrieve their lumen, but how, for the third one, which has not a really bright lumen and is not completely surrounded with CTL, we do not. That is one limitation of the method.

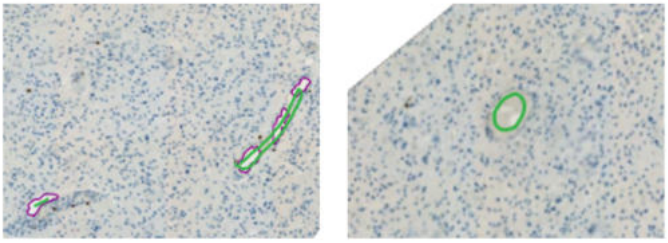

Figure 8: Third scene samples. Borders in red, derived lumen in blue, lumen in purple and ground truth in green

The third sceme is a special case as it features very little CTL. Such that we only take the maxima into account. Obvious bright and opened vessels are correctly retrieve, but not when the lumen is too small or partly stained like on the right. The parameters would be to sensitive to the overall background, had we tried to segment these.

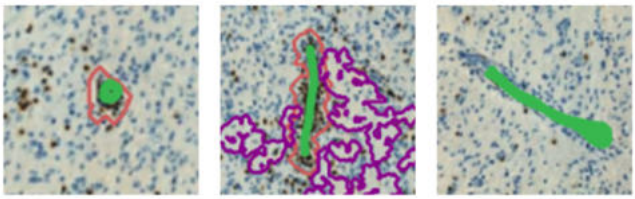

Figure 9: Fourth scene samples. Borders in red, derived lumen in blue, lumen in purple and ground truth in green

The last scene only features closed vessels. Notice how – in the center – the whole lumen retrieving part of the method is clueless and should be ignored in such case. To that end, one can simply set the parameter `HP_THRESHOLD` above 1, to disable the lumen detection branch. Pure closed vessels detection is easier than pure opened vessels detection however, except that the method is bound to miss closed vessels that are not surrounded with CTL, like the one on the right.
Below we give the total results on the four scenes, per scene.

Scenes	True positive	False positive	False negative	Precision	Recall
1	2	22	14	0.08	0.125
2	4	1	0	0.8	1
3	6	1	9	0.86	0.4
4	10	2	10	0.83	0.5

Table 1: total results

5. CODE AND DATA AVAILABILITY

For further details, parameters' values used for each slide are given in appendix A. Moreover, all code and data used, full-sized results as well as a demonstrative notebook are available on the following repository.

6. CONCLUSION

We proposed a method to automatically segment blood vessels on CD3-stained WSI in the case of a CTL diffusion description of glioblastoma. It must be acknowledged that results are not good. Not only does the method fail to completely and accurately detect blood vessels in various conditions, but it requires some parameter tuning as well. This could be expected since well performing state-of-the-art methods use much more precise staining methods. Obviously, all further improvement should be assessed on a much larger amount of annotated data - as it is hard to draw definitive conclusions with the current testing data. Hopefully, there are several opportunities for improvement.
First, a fair part of the poor results either comes from a insufficient resolution or from a inner-slide variability that cannot be resolved by the current parameters, which we kept sparse on purpose. It would probably be beneficial to work at the native resolution rather than the current one-tenth, and secondly, it appears necessary to make use of a pre-clustering method to adapt parameters' values given the stain local saturation, cell density, or related criteria. Some extensive clustering methods have already been proposed for such cases, such as the very recently proposed comprehensive analysis tool by *Warshold & al.*[16] and that we could take inspiration from.
It may also be interesting to adapt new purposely more generalized methods based on staining transfer such as the one proposed by *Hamidinekoo & al.*[15] that built a bridge between standard H&E staining and highly specialized anti-ERG one for blood vessel segmentation, this time from anti-CD3 staining to other staining methods well suited for blood vessel segmentation, such as anti-CD31, anti-CD34 or anti-ERG mentioned here.

REFERENCES

[1] A. Saste, J. Arias-Stella, and P. Kuriakose. “Progression of a hepatosplenic gamma delta T-cell leukemia/lymphoma on hyperCVAD/MTX and ara-C: literature review and our institutional treatment approach”. In: *Clin Case Rep* 4.1 (Jan. 2016), pp. 67–71.

[2] Quinn T Ostrom et al. “CBTRUS statistical report: primary brain and central nervous system tumors diagnosed in the United States in 2008-2012”. In: *Neuro-oncology* 17.suppl_4 (2015), pp. iv1–iv62.

[3] Miranda W. Yu and Daniela F. Quail. “Immunotherapy for Glioblastoma: Current Progress and Challenges”. In: *Frontiers in Immunology* 12 (2021). ISSN: 1664-3224. DOI: 10.3389/fimmu.2021.676301. URL: https://www.frontiersin.org/articles/10.3389/fimmu.2021.676301.

[4] Parmida Ghahremani et al. “DeepLIIF: An Online Platform for Quantification of Clinical Pathology Slides”. In: *Proceedings of the IEEE/CVF Conference on Computer Vision and Pattern Recognition (CVPR)*. June 2022, pp. 21399–21405.

[5] C Higgins. “Applications and challenges of digital pathology and whole slide imaging”. In: *Biotechnic & Histochemistry* 90.5 (2015). PMID: 25978139, pp. 341–347. DOI: 10.3109/10520295.2015.1044566. URL: https://doi.org/10.3109/10520295.2015.1044566.

[6] Xintong Li et al. “A comprehensive review of computer-aided whole-slide image analysis: from datasets to feature extraction, segmentation, classification and detection approaches”. In: *Artificial Intelligence Review* 55.6 (Aug. 2022), pp. 4809–4878. ISSN: 1573-7462. DOI: 10.1007/s10462-021-10121-0. URL: https://doi.org/10.1007/s10462-021-10121-0.

[7] Faliu Yi et al. “Microvessel prediction in H&E Stained Pathology Images using fully convolutional neural networks”. en. In: *BMC Bioinformatics* 19.1 (Feb. 2018), p. 64.

[8] Massimo Salvi et al. “Karpinski Score under Digital Investigation: A Fully Automated Segmentation Algorithm to Identify Vascular and Stromal Injury of Donors’ Kidneys”. In: *Electronics* 9.10 (2020). ISSN: 2079-9292. DOI: 10.3390/electronics9101644. URL: https://www.mdpi.com/2079-9292/9/10/1644.

[9] Faiza Bukenya et al. “An automated method for segmentation and quantification of blood vessels in histology images”. In: *Microvascular Research* 128 (2020), p. 103928. ISSN: 0026-2862. DOI: https://doi.org/10.1016/j.mvr.2019.103928. URL: https://www.sciencedirect.com/science/article/pii/S0026286218301262.

[10] Dorin Comaniciu and Peter Meer. “Mean Shift: A Robust Approach Toward Feature Space Analysis”. In: *IEEE Trans. Pattern Anal. Mach. Intell.* 24 (2002), pp. 603–619.

[11] Jonathan Charles Goddard et al. “A computer image analysis system for microvessel density measurement in solid tumours”. en. In: *Angiogenesis* 5.1-2 (2002), pp. 15–20.

[12] Maria-Milagro Fernández-Carrobles et al. “A morphometric tool applied to angiogenesis research based on vessel segmentation”. In: *Diagnostic Pathology* 8.1 (Sept. 2013), S20. ISSN: 1746-1596. DOI: 10.1186/1746-1596-8-S1-S20. URL: https://doi.org/10.1186/1746-1596-8-S1-S20.

[13] C C Reyes-Aldasoro et al. “An automatic algorithm for the segmentation and morphological analysis of microvessels in immunostained histological tumour sections”. en. In: *J. Microsc.* 242.3 (June 2011), pp. 262–278.

[14] Chi-Hsuan Tsou et al. “A Heuristic Framework for Image Filtering and Segmentation: Application to Blood Vessel Immunohistochemistry”. In: *Analytical Cellular Pathology* 2015 (Dec. 2015), p. 589158. ISSN: 2210-7177. DOI: 10.1155/2015/589158. URL: https://doi.org/10.1155/2015/589158.

[15] Azam Hamidinekoo et al. “Automated Quantification Of Blood Microvessels In Hematoxylin And Eosin Whole Slide Images”. In: *Proceedings of the MICCAI Workshop on Computational Pathology*. Ed. by Manfredo Atzori et al. Vol. 156. Proceedings of Machine Learning Research. PMLR, 27 Sep 2021, pp. 94–104. URL: https://proceedings.mlr.press/v156/hamidinekoo21a.html.

[16] Simon Warchol et al. “Visinity: Visual spatial neighborhood analysis for multiplexed tissue imaging data”. en. In: *IEEE Trans. Vis. Comput. Graph.* PP (Sept. 2022), pp. 1–11.

APPENDIX A. TABLES OF PARAMETERS

LP_THRESHOLD	75
HP_THRESHOLD	1.1
MIN_AREA	250
MAX_AREA	50000
TILE_SIZE	512

Table 1: 0_6 *(first scene) parameters*

LP_THRESHOLD	75
HP_THRESHOLD	0.7
MIN_AREA	200
MAX_AREA	50000
TILE_SIZE	512

Table 2: 2_2 *(second scene) parameters*

LP_THRESHOLD	35
HP_THRESHOLD	0.95
MIN_AREA	150
MAX_AREA	50000
TILE_SIZE	512

Table 3: 4_1 *(third scene) parameters*

LP_THRESHOLD	100
HP_THRESHOLD	0.99
MIN_AREA	200
MAX_AREA	50000
TILE_SIZE	512

Table 4: 5_1 *(fourth scene) parameters*

,